# Two-component galaxy models: the effect of density profile at large radii on the phase-space consistency

# Luca Ciotti & Lucia Morganti\*

Astronomy Department, University of Bologna, via Ranzani 1, 40127 Bologna, Italy

Submitted, October 1, 2008. Accepted version, November 3, 2008.

#### ABSTRACT

It is well known that the density and anisotropy profile in the inner regions of a stellar system with positive phase-space distribution function are not fully independent. Here we study the interplay between density profile and orbital anisotropy at large radii in physically admissible (consistent) stellar systems. The analysis is carried out by using two-component  $(n-\gamma,\gamma_1)$  spherical self-consistent galaxy models, in which one density distribution follows a generalized  $\gamma$  profile with external logarithmic slope n, and the other a standard  $\gamma_1$  profile (with external slope 4). The two density components have different "core" radii, the orbital anisotropy is controlled with the Osipkov-Merritt recipe, and for simplicity we assume that the mass of the  $\gamma_1$  component dominates the total potential everywhere. The necessary and sufficient conditions for phase-space consistency are determined analytically, also in presence of a dominant massive central black hole, and the analytical phase-space distribution function of  $(n-\gamma,1)$  models, and of  $n-\gamma$  models with a central black hole, is derived for  $\gamma=0,1,2$ . It is found that the density slope in the external regions of a stellar system can play an important role in determining the amount of admissible anisotropy: in particular, for fixed density slopes in the central regions, systems with a steeper external density profile can support more radial anisotropy than externally flatter models. This is quantified by an inequality formally identical to the "cusp slope-central anisotropy" theorem (An & Evans 2006), relating at all radii (and not just at the center) the density logarithmic slope and the anisotropy indicator in all Osipkov-Merritt systems.

**Key words:** stellar dynamics – galaxies: ellipticals – dark matter – black holes

### 1 INTRODUCTION

Observationally it is well established that elliptical galaxies have dark matter halos, and also host central supermassive black holes. These empirical facts motivate the study of multi-component dynamical models. When studying dynamical models of stellar systems (single or multicomponent), the minimal requirement to be met by a physically acceptable model is the positivity of the phase-space distribution function (DF) of each distinct component. A model satisfying this essential requirement (which is much weaker than stability, but stronger than the fact that the Jeans equations have a physically acceptable solution) is called *consistent*; moreover, when the total gravitational potential is determined by the total density profile through the Poisson equation, the model is called self-consistent. In other words, we call self-consistent a consistent selfgravitating system.

 $^\star$  Current address: Max-Planck-Institut für Ex. Physik, Giessenbachstraße, D-85741 Garching, Germany

Two general strategies can be used to construct a (self) consistent model, or check whether a proposed model is (self) consistent: they are commonly referred to as the "fto- $\rho$ " and the " $\rho$ -to-f" approaches, where f is the model DF (e.g., see Bertin 2000, Binney & Tremaine 2008). An example of the first approach is the survey of self-consistent two-component galaxy models carried out by Bertin and co-workers, where the stellar and dark matter components are described by two DFs of the  $f_{\infty}$  family (e.g., Bertin & Stiavelli 1984, Bertin et al. 1992); other well known examples are the King (1966) models and the  $f_{\nu}$  models (Bertin & Trenti 2003). Unfortunately, the resulting spatial densities obtained by solving the associated Poisson equation are in general not expressible in terms of simple or even known functions, and so only numerical investigations are usually feasible. In the " $\rho$ -to-f" approach the density distribution is given, and specific assumptions about the model internal dynamics are made; in special cases inversion formulae from the density to the DF can be obtained, usually in integral form or series expansion (see, e.g., Fricke 1952, Lynden-Bell 1962, Osipkov 1979, Merritt 1985, hereafter OM; Dejonghe

1986, 1987; Cuddeford 1991; Hunter & Qian 1993, Ciotti & Bertin 2005). In particular, in order to recover the DF of spherical models with orbital anisotropy, the OM technique has been developed from the Eddington (1916) inversion for isotropic systems, and widely used to study one and two-component models (see, e.g., Ciotti & Pellegrini 1992, hereafter CP92; Hiotelis 1994; Carollo et al. 1995; Ciotti & Lanzoni 1997; Ciotti 1996, 1999, hereafter C96, C99; Baes & Dejonghe 2004; Buyle et al. 2007). We remark that the OM parameterization is not necessarily the best description of real systems, however its simplicity and the fact that it captures the main features of models of galaxy formation, that are generally found nearly isotropic at the center and increasingly radially anisotropic in the outer envelope (e.g., van Albada 1982; Trenti, Bertin & van Albada 2005; Nipoti, Londrillo & Ciotti 2006; Binney & Tremaine 2008. But see Cuesta et al. 2008 and references therein), make it the natural choice for investigations as that presented in this paper.

In many cases, the difficulties inherent in the operation of recovering analytically the DF prevent a simple consistency analysis, and phase-space positivity must be investigated by numerical inspection of the inversion integral. In these cases the reasons underlying consistency or inconsistency of a proposed model tend to be obscured by the numerical nature of the solution. Fortunately, informations about consistency of multi-component OM systems can be obtained without recovering their DF, following the procedure described in CP92. This method uses the radial density profile of each component and the total potential of the system, and gives necessary and sufficient conditions for (self) consistency. Moreover, since only spatial differentiation and inequality checks are required, this method is best suited for analytical investigations. For example, C96 and C99 applied the CP92 technique to the general family of two-component, spherically symmetric and radially anisotropic  $(\gamma_1, \gamma_2)$  models. This family is made of the superposition of two  $\gamma$  models (Dehnen 1993, Tremaine et al. 1994) with different total masses, scale-lengths, inner density slopes, and OM radially anisotropic velocity dispersions. The possibility to investigate the combined effects of radial anisotropy and inner density slope on multi-component systems made the study of  $(\gamma_1, \gamma_2)$  models interesting, as it is well known that the inner density profile sets important constraints on the amount of admissible radial anisotropy (e.g., Richstone & Tremaine 1984), and indeed in C96 and C99 analytical limitations on anisotropy as a function of the density slopes  $\gamma_1$  and  $\gamma_2$  were obtained. These models clarified the reasons behind the numerical findings of CP92, i.e. the difficulty of consistently superimposing a centrally peaked distribution such as the de Vaucouleurs (1948) profile to a centrally flat one, such as the King (1972) or quasi-isothermal density profile (even in the isotropic case). In fact, it was shown that the DF of the  $\gamma_1$  component in isotropic  $(\gamma_1, \gamma_2)$  models is nowhere negative, independently of the mass and concentration of the  $\gamma_2$ component, whenever  $0 \le \gamma_2 \le \gamma_1$  and  $1 \le \gamma_1 < 3$ . On the contrary, a  $\gamma_1 = 0$  component becomes inconsistent when adding a  $\gamma_2 = 1$  halo with a small core radius. Thus, in two-component isotropic models, the component with the steeper central density distribution is usually the most robust against inconsistency. More recently, the importance of the central density slope in limiting the amount of possible radial anisotropy has also been quantified with the so called

"cusp slope-central anisotropy" theorem (An & Evans 2006, hereafter AE06; see also eq. [28] in de Bruijne et al. 1996).

The previous investigations left however unexplored the importance of the external density slope in determining the model consistency. In fact, the phase-space density cannot be identified, in general, with any specific spatial position in the system, as (for example) stars of a given energy can span a large range of radial positions<sup>1</sup> (systems made of circular orbits are an obvious exception). Therefore also the external regions of a density distribution can be important in limiting the maximum allowable anisotropy, but the  $(\gamma_1, \gamma_2)$  models are of no help in the study of this issue, because the external density profiles of both components all decrease as  $r^{-4}$ . For these reasons here we focus on the phase-space properties of  $n-\gamma$  models, i.e. models similar to the standard  $\gamma$ models in the inner regions, but with a density profile proportional to  $r^{-n}$  (instead of  $r^{-4}$ ) in the external regions; remarkably, several properties of  $n-\gamma$  models can be obtained from those of  $\gamma$  models by differentiation with respect to their scale–length. In this notation, the 4- $\gamma$  models coincide with the standard  $\gamma$  models. We also study the larger class of  $(n-\gamma,\gamma_1)$  models, i.e. two-component systems in which a  $\gamma_1$  halo is added to a n- $\gamma$  component. Thus, here we further explore the trends emerged in CP92, C96, and C99, determining the limits imposed by phase-space consistency on the parameters describing  $(n-\gamma,\gamma_1)$  models, and  $n-\gamma$  models with a central BH [hereafter  $(n-\gamma, BH)$  models], with particular focus on the effects of the external slope parameter n. In specific cases (that we call halo-dominated models), the calculations are performed under the assumption that the mass of the halo component (or of the central BH) is dominant over the mass of the visible one. This assumption is mainly motivated by mathematical simplicity (see also Sect. 4), although this is not the only reason. In fact, for any given two-component model, it is expected that the DF properties are bracketed by those of the one component model and by those of the halo-dominated model (corresponding to the formal case of an infinite halo mass). Of course, while the case of dark matter dominated systems can be considered a viable representation of some real astrophysical systems, the case of a dominant BH is less natural, and it just gives the strongest possible limitations for consistency of systems with a central BH.

The paper is organized as follows. In Section 2 we briefly review the technique developed in CP92, and we prove that the necessary condition for consistency derived in CP92 for OM systems can be rewritten *exactly* as the AE06 "cusp slope-central anisotropy" theorem, holding however at all radii and not just at the center. In Section 3 the one and two—

<sup>&</sup>lt;sup>1</sup> Incidentally, this implies that the use of  $\rho/\sigma^3$  as a proxy for phase–space density, where  $\sigma$  is the local value of the velocity dispersion, has no assignable meaning without an appropriate discussion. For example, in power–law isotropic systems with  $\rho \propto r^{-\gamma}$ , because the functions  $\rho/\sigma^3 \propto r^{\frac{\gamma-6}{2}}$  (for  $\gamma>1$ ) and phase–space density  $f(\mathcal{E}) \propto \mathcal{E}^{\frac{6-\gamma}{2(\gamma-2)}}$  (for  $\gamma>2$ , where  $\mathcal{E}=-E$  is the so–called relative energy, see Sect. 4 and Baes et al. 2005) are both power laws with respect to their arguments, the exponents are related in a simple way. However, the converse statement is not true: for example, in the Plummer (1911) sphere  $f(\mathcal{E}) \propto \mathcal{E}^{7/2}$  is a power law at all energies, but  $\rho/\sigma^3$  is not a power law of radius.

component n- $\gamma$  models are introduced, and the necessary and sufficient conditions imposed on the model parameters by phase–space consistency are derived for different values of the logarithmic density slope n. In Section 4 the DF of the n- $\gamma$  component of halo-dominated (n- $\gamma$ ,1) models with  $\gamma = 0, 1, 2$ , and of similar models with a dominant central BH, are derived explicitly for arbitrary (but integer) values of n, and the true boundaries of the consistency region in the parameter space are obtained. The main results of the investigation are summarized in Section 5. Finally, in the Appendix an easy method to solve analytically the Jeans equations in the general OM case for the wider class of  $(n_1$ - $\gamma_1, n_2$ - $\gamma_2)$  models is presented.

## 2 THE CONSISTENCY OF MULTI-COMPONENT OM SYSTEMS

A stellar system made of the sum of the density components  $\rho_k$  is called consistent if each DF  $(f_k)$  is non-negative over the whole accessible phase-space; a consistent self-gravitating system is called self-consistent. The technique developed in CP92 permits us to check whether the DF of a multi-component spherical system, where the orbital anisotropy of each component is modeled according to the OM parameterization, is positive; in practice, only information about the radial trend of each density component and of the total integrated mass are used. In the OM formulation the DF of each component is obtained assuming  $f_k = f_k(Q_k)$ , with

$$Q_{\mathbf{k}} = \mathcal{E} - \frac{J^2}{2r_{\mathbf{ak}}^2},\tag{1}$$

where  $\mathcal{E}$  and J are respectively the relative energy and the angular momentum modulus per unit mass,  $r_{\rm ak}$  is the so-called anisotropy radius, and  $f_{\rm k}=0$  for  $Q_{\rm k}\leq 0$  (e.g. see Binney & Tremaine 2008). The velocity dispersion tensor associated with eq. (1) is characterized by radial anisotropy increasing with the radius r, while in the limit  $r_{\rm ak}\to\infty$  the system becomes globally isotropic. As well known, the DF of the density component  $\rho_{\rm k}$  is given by

$$f_{k}(Q_{k}) = \frac{1}{\sqrt{8}\pi^{2}} \frac{d}{dQ_{k}} \int_{0}^{Q_{k}} \frac{d\varrho_{k}}{d\Psi_{T}} \frac{d\Psi_{T}}{\sqrt{Q_{k} - \Psi_{T}}}$$

$$= \frac{1}{\sqrt{8}\pi^{2}} \int_{0}^{Q_{k}} \frac{d^{2}\varrho_{k}}{d\Psi_{T}^{2}} \frac{d\Psi_{T}}{\sqrt{Q_{k} - \Psi_{T}}},$$
(2)

where the augmented density is

$$\varrho_{\mathbf{k}}(r) \equiv \left(1 + \frac{r^2}{r_{\mathbf{a}\mathbf{k}}^2}\right) \rho_{\mathbf{k}}(r),\tag{3}$$

 $\Psi_{\rm T}(r) = \sum_k \Psi_{\rm k}(r)$  is the total relative potential,  $0 \le Q_{\rm k} \le \Psi_{\rm T}(0)$ , and in the integrals above it is assumed that the radius is eliminated from  $\varrho_{\rm k}$  in favour of  $\Psi_{\rm T}$ . It can be proved that the second equivalence in eq. (2) holds for untruncated systems with finite total mass, as the models discussed here.

# 2.1 Necessary and sufficient conditions for consistency

Quite obviously, only a very limited number of density profiles among those expressible in analytic form admit an explicit DF, so that the study of phase–space consistency would appear restricted to such rare cases when conducted analytically, while all the remaining cases should be investigated numerically. Fortunately this is not true, as the CP92 technique is based on the verification (numerical or analytical) of the following

**Theorem:** A necessary condition (NC) for the non-negativity of  $f_k$  is

$$\frac{d\varrho_{\mathbf{k}}(r)}{dr} \le 0, \quad 0 \le r \le \infty. \tag{4}$$

If the NC is satisfied, a strong sufficient condition (SSC) for the non–negativity of  $f_{\bf k}$  is

$$\frac{d}{dr} \left[ \frac{d\varrho_{\mathbf{k}}(r)}{dr} \frac{r^2 \sqrt{\Psi_{\mathbf{T}}(r)}}{M_{\mathbf{T}}(r)} \right] \ge 0, \quad 0 \le r \le \infty.$$
 (5)

Finally, a weak sufficient condition (WSC) for the non negativity of  $f_{\mathbf{k}}$  is

$$\frac{d}{dr} \left[ \frac{d\varrho_{\mathbf{k}}(r)}{dr} \frac{r^2}{M_{\mathrm{T}}(r)} \right] \ge 0, \quad 0 \le r \le \infty.$$
 (6)

**Proof**: See CP92, C96, C99.

The first consideration that follows from the conditions above is that the violation of the NC is connected only to the radial behavior of the augmented density  $\varrho_k$ , and so this condition applies independently of any other density component of the model. Obviously, a model failing the NC is certainly inconsistent, while a model satisfying the NC may be inconsistent, i.e. the  $f_k$  may be negative even for values of model parameters allowed by the NC. The second consideration is that a model satisfying the WSC (or the more restrictive SSC) is certainly consistent, while a model failing the WSC (SSC) may be consistent. Therefore the consistency of an OM model satisfying the NC and failing the WSC (or the SSC) can be proved only by direct inspection of its DF.

### 2.1.1 A density slope-OM anisotropy inequality

The NC can be recast into a simple inequality between the value of the density slope

$$\gamma(r) \equiv -\frac{d\ln\rho}{d\ln r} \tag{7}$$

and the value of the orbital anisotropy indicator

$$\beta(r) \equiv 1 - \frac{\sigma_{\rm t}^2}{2\sigma_{\rm r}^2} = \frac{r^2}{r^2 + r_{\rm a}^2}$$
 (8)

that must hold at each radius for consistent OM systems. In the expression above  $\sigma_{\rm r}^2$  and  $\sigma_{\rm t}^2$  are the radial and tangential components of the velocity dispersion tensor of the system (e.g. Binney & Tremaine 2008), and in the following proof we restrict to natural systems, i.e. systems with monotonically decreasing density profile, so that  $\gamma(r)>0$ . The proof is trivial: in fact, it suffices to express the NC in terms of the logarithmic density slope as

$$\frac{2}{\gamma(r)} - \frac{r^2}{r^2 + r_a^2} \le 0,\tag{9}$$

and from eq. (8) one obtains the necessary condition

$$\gamma(r) \ge 2\beta(r),\tag{10}$$

# 4 Ciotti & Morganti

which must be verified by each OM component of a consistent multi-component system. Curiously, The condition above is formally *identical* to the inequality appearing in the "cusp slope-central anisotropy" theorem derived in AE06. This latter theorem was proved by using constant anisotropy systems (i.e.,  $\beta(r) = \beta$ , and in this case as well the inequality above holds at all radii in consistent models. See eq. [10] in AE06), and then it was convincingly argued that the inequality it holds asymptotically for the central regions of spherical systems with generic anisotropy distribution.

In the specific case of n- $\gamma$  density distributions (see eq. [18]), the logarithmic density slope

$$\gamma(r) = \frac{\gamma + ns}{1+s}, \qquad s = \frac{r}{r_c},\tag{11}$$

and therefore eq. (10) shows that in general the NC is satisfied near the center of OM systems (where  $\beta=0$  and  $\gamma(r)=\gamma$ ), and at large radii (where  $\beta=1$  and  $\gamma(r)=n\geq 3$ ), while critical behaviors may be expected at intermediate radii (see Sect. 4).

# 2.2 Classification of phase-space inconsistency as a function of the anisotropy radius

Interestingly (but not unexpectedly) the particular functional form of the augmented density characteristic of OM parametrization, limits the possible manifestations of phase–space inconsistency to few general cases, that can be illustrated as follows. From eqs. (2)-(3) it is apparent that the DF of each density component can be written as

$$f(Q) = f_i(Q) + \frac{f_a(Q)}{r_a^2},$$
 (12)

where  $f_i$  is the DF of the considered density component in the isotropic case (for simplicity, from now on we avoid the use of the subscript k). Let  $A_+$  be the subset of phase–space defined by the property that  $f_i$  is positive  $\forall Q \in A_+$ . Then, from eq. (12) a first condition to be satisfied for consistency is

$$r_{\rm a} \ge r_{\rm a}^- \equiv \sqrt{\max\left\{0, \sup\left[-\frac{f_{\rm a}(Q)}{f_{\rm i}(Q)}\right]_{Q \in A_+}\right\}}.$$
 (13)

Obviously, when  $f_i > 0$  over all the accessible phase–space (the common situation for realistic density distributions), inequality (13) is also the *only* condition to be satisfied for the model consistency, and there is at most a lower bound for the anisotropy radius. For example this is the case for the families of one–component anisotropic  $\gamma$  models (C99) and Sersic (1968) models (Ciotti 1991).

When the complement of  $A_+$  is not empty, i.e.  $f_i < 0$  over some region  $A_-$  of the accessible phase–space, a second inequality again derived from eq. (12) must be verified for consistency:

$$r_{\rm a} \le r_{\rm a}^+ \equiv \sqrt{\inf \left[\frac{f_{\rm a}(Q)}{|f_{\rm i}(Q)|}\right]_{Q \in A_-}}$$
 (14)

Therefore, if there exists some  $Q \in A_{-}$  for which  $f_a < 0$ , then the proposed model is inconsistent<sup>2</sup>. If  $f_a$  is positive

over  $A_-$ , from conditions (13)-(14) it follows that  $r_a^- < r_a < r_a^+$  for OM consistency, so that if  $r_a^+ < r_a^-$  the proposed model is inconsistent. Note that formally *identical* considerations hold when discussing the inequalities (4) and (6), because from eq. (3) it follows that the NC and WSC can be written in the same functional form of eq. (12): of course, in these cases the sets  $A_+$  and  $A_-$  are to be intended as subsets of the radial range  $0 \le r \le \infty$ .

In the following Section, after presenting the one and two–component n- $\gamma$  models, the necessary and sufficient conditions for model consistency will be derived, also for the case of n- $\gamma$  models with a massive central black hole.

# 3 THE ONE AND TWO–COMPONENT n- $\gamma$ MODELS

The one–component n- $\gamma$  models are a natural generalization of the widely explored family of the so–called  $\gamma$  models (Dehnen 1993, Tremaine et al. 1994), whose density, cumulative mass within r, and relative potential are given by

$$\rho(r) = \frac{3 - \gamma}{4\pi} \frac{Mr_{\rm c}}{r^{\gamma} (r_{\rm c} + r)^{4 - \gamma}},\tag{15}$$

$$M(r) = M \times \left(\frac{r}{r_{\rm c} + r}\right)^{3 - \gamma},\tag{16}$$

$$\Psi(r) = \frac{GM}{r_{\rm c}} \left\{ \frac{1}{(2-\gamma)} \left[ 1 - \left(\frac{r}{r+r_{\rm c}}\right)^{2-\gamma} \right] \right.$$

$$\left. \ln \frac{r+r_{\rm c}}{r}, \quad (\gamma=2), \right.$$

$$(17)$$

respectively.

In the n- $\gamma$  models the logarithmic density slope for  $r \gg r_{\rm c}$  is not 4, but it is a free parameter n>3 (to ensure that their total mass is finite), so that these density profiles belong to the family considered by Zhao (1996). In the following, in order to exploit a useful analytical property of the n- $\gamma$  density profiles, we will often assume n restricted to integer values  $\geq 4$ . In fact, the generic density profile of a n- $\gamma$  model is given by

$$\rho_n(r) \equiv \frac{Mr_c^{n-3}}{4\pi B(3-\gamma, n-3)r^{\gamma}(r_c+r)^{n-\gamma}}$$

$$= \frac{r_c^{n-3}(-1)^n}{\Gamma(n-3)} \frac{d^{n-4}}{dr_c^{n-4}} \frac{\rho(r)}{r_c},$$
(18)

where M is the total mass of the density distribution,  $\mathrm{B}(x,y) = \Gamma(x)\Gamma(y)/\Gamma(x+y)$  and  $\Gamma(x)$  are the complete Euler beta and gamma functions, respectively, and the first expression holds for any real number n>3. The second expression, based on repeated differentiation of eq. (15) with respect to  $r_{\rm c}$ , holds instead for integer  $n\geq 4$ . Of course, for n=4 the standard  $\gamma$  model density profile is recovered. The radial behaviour of  $\rho_n(r)$  is shown in Fig. 1 (top panel) for n-1 models with increasing n. In the bottom panel we show the corresponding logarithmic density slopes, calculated accordingly to eq. (11). In particular, it is apparent how the inner slope is  $\gamma$  (for  $r\lesssim \gamma r_{\rm c}/n$ ), and the external is n (for  $r\gtrsim r_{\rm c}$ ). As a consequence, while the density profile outside  $r_{\rm c}$  becomes more and more steep at increasing n, the innermost region where the density slope is  $\gamma$  contracts near the

 $<sup>^2</sup>$  In C99 and Ciotti (2000) it is erroneously stated that the model is inconsistent if  $f_{\rm a}<0~\forall Q\in A_-.$  All the results presented therein are however correct.

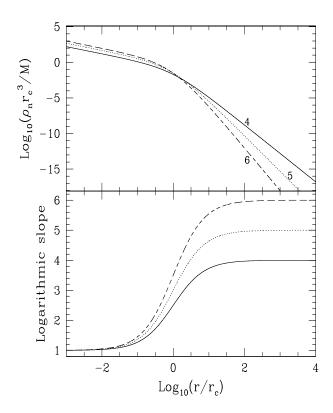


**Figure 1.** The normalized density profile  $\rho_n$  of the n-1 model (top panel), and its logarithmic slope (eq. [11], bottom panel), for n = 4, 5, and 6.

center. As anticipated, the possibility to write the density  $\rho_n$  as a derivative with respect to the scale–length  $r_{\rm c}$  provides an easy way to determine analytical properties of the n- $\gamma$  models for n integer. Indeed, since the density enters linearly in the integrals of the total mass inside the radius r and of the potential, from eq. (18) it follows that

$$M_n(r) = \frac{r_c^{n-3}(-1)^n}{\Gamma(n-3)} \frac{d^{n-4}}{dr_c^{n-4}} \frac{M(r)}{r_c},$$
(19)

$$\Psi_n(r) = \frac{r_c^{n-3}(-1)^n}{\Gamma(n-3)} \frac{d^{n-4}}{dr_c^{n-4}} \frac{\Psi(r)}{r_c}.$$
 (20)

Instead, when n is not at integer,  $M_n$  and  $\Psi_n$  are in general given by hypergeometric  ${}_2F_1$  functions. Expressions similar to eqs. (19)-(20) hold for any quantity that can be written as a linear functional of  $\rho_n$ , so that the surface density profile of n- $\gamma$  models with n integer can be obtained by repeated differentiation of the surface density profile of  $\gamma$  models (when analytically available, e.g. see Binney & Merrifield 1998). This property will be exploited in Section 4 to obtain the explicit DF of halo dominated (n- $\gamma$ , $\gamma_1$ ) models; moreover, in Appendix B we show how quadratic functionals of  $\rho_n$  (such as the gravitational energy and the velocity dispersions) can be also evaluated by using repeated differentiation with respect to  $r_c$ .

We are now in the position to introduce the twocomponent models used in this work. The most general family of two-component n- $\gamma$  models, i.e. the  $(n_1$ - $\gamma_1, n_2$ - $\gamma_2)$ models, is made of the superposition of two n- $\gamma$  models with different total masses, scale-lengths, internal and external density slopes, and finally two different anisotropy radii. For simplicity here we restrict to the case of  $(n-\gamma,\gamma_1)$  models, where the "halo" density distribution is a standard  $\gamma_1$  model: we note however that some of the presented results can be generalized without much effort to the family of  $(n_1-\gamma_1,n_2 \gamma_2$ ) models (see Appendix B). In the following, the total mass  $M_1$  and the characteristic scale-length  $r_1$  of the  $\gamma_1$  halo are adopted as normalization constants, so that the physical scales for density and potential are given by  $\rho_{\rm N}=M_1/r_1^3$ and  $\Psi_{\rm N} = GM_1/r_1$ , while we define  $s \equiv r/r_1$ ,  $\xi \equiv r_{\rm c}/r_1$ ,  $\mu \equiv M/M_1$ . With this choice, the  $(n-\gamma,\gamma_1)$  models are structurally determined by fixing the four independent parameters  $(M_1, r_1, \mu, \xi)$ , with the obvious conditions  $\mu \geq 0$  and  $\xi > 0$ . We conclude this introductory discussion by noticing that, for reasons that will become apparent in Section 3.2 and 4, the present normalization differs from that adopted in C99, where the normalization mass and scale-length were those of the first component.

# 3.1 The necessary and sufficient conditions for one–component n- $\gamma$ models

Before discussing the case of the two–component models, we consider the NC for anisotropic n- $\gamma$  models, in order to determine analytically a critical value for the anisotropy radius such that a higher degree of radial OM anisotropy (i.e., a smaller  $r_{\rm a}$ ) would produce a negative DF for some permitted value of Q. We recall that the obtained anisotropy limit holds also when a second component is added (see Section 2), so that the present discussion is fully general. Moreover, we note that as the NC involves only the density distribution under scrutiny, we can use the first expression in eq. (18), and the following results hold for any n > 3, not necessarily limited to integers. In the following the unit mass and unit length are the total mass M and the scale–length  $r_{\rm c}$  of the n- $\gamma$  model, with  $s_{\rm a} = r_{\rm a}/r_{\rm c}$ .

In C99 the analytical expression for the critical  $s_{\rm a}(\gamma)$  was obtained for the whole family of  $\gamma$ -models, and here we derive its generalization  $s_{\rm a}(\gamma,n)$ . In fact, eq. (A1) shows that for  $2 \leq \gamma < 3$  and n > 3 the NC is satisfied for  $s_{\rm a} \geq 0$ , and the result of C99 is now obtained as the particular case for n = 4. In other words, the NC leaves open the possibility of making n- $\gamma$  models with  $\gamma \geq 2$  using radial orbits only. In the range  $0 \leq \gamma < 2$  the NC requires instead that

$$s_{\rm a} \ge s_{\rm M} \sqrt{\frac{2 - \gamma - (n - 2)s_{\rm M}}{\gamma + ns_{\rm M}}},\tag{21}$$

where the explicit expression of  $s_{\rm M}(n,\gamma)$  is given by eq. (A2), and the inequality above reduces to eq. (13) of C99 when n=4. The NC then proves that n- $\gamma$  models with  $0 \le \gamma < 2$  cannot be made of radial orbits only, independently of the value of the external slope n, and of the presence of any possible second component. This result extends the list of cases for which it has been proved that a density cusp shallower than  $r^{-2}$  cannot be supported by radial orbits only (Richstone & Tremaine 1984, CP92, C99, AE06). In Fig. 2 the lower bound for the anisotropy radius given in eq. (21) is shown with the solid lines as a function of  $\gamma$  for n=4,5,6: n- $\gamma$  models (one or multi–component) with the pair  $(s_{\rm a},\gamma)$  in the nearly triangular region under the solid

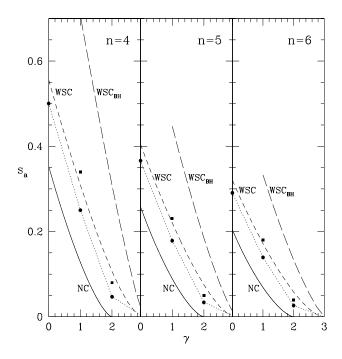


Figure 2. Consistency limits on  $s_{\rm a}=r_{\rm a}/r_{\rm c}$  as a function of  $\gamma$  in one–component n- $\gamma$  models, for n=4,5,6. The NC limit is represented by the solid lines: all models with the pair  $(s_{\rm a},\gamma)$  in the triangular region below them are inconsistent. The dashed lines mark the WSC limit: all points above these lines correspond to consistent one–component n- $\gamma$  models. For  $\gamma=0,1,2$ , the filled circles joined by the dotted line represent the more accurate limits obtained from the SSC. For the black-hole dominated (n- $\gamma$ ,BH) models the long-dashed lines (interrupted for  $\gamma<1$ , see Section 3.2), are the lower limit on  $s_{\rm a}$  given by the WSC, while the solid squares are the true limits derived from the DF.

curves are inconsistent. In particular, for fixed  $\gamma$  an increase of n produces a decrease of the minimum  $s_{\rm a}$ , i.e. we have here a first indication that a steepening of the density profile in the external regions of a system with fixed inner density slope can be effective in increasing the maximum amount of sustainable radial anisotropy. This behaviour is quantified by substitution in eq. (21) of the asymptotic expansion for  $n \to \infty$  of  $s_{\rm M}(n,\gamma)$  in eq. (A2):

$$s_{\rm M}(n,\gamma) = \frac{1 - 2\gamma + \sqrt{1 + 4\gamma}}{2n} + {\rm O}(n^{-2}).$$
 (22)

As often happens in asymptotic analysis, even if the expansion above holds in principle only for very large values of n, the substitution of (22) in (21) leads to percentual errors on  $s_a$  less than 22%, 14%, and 10% for n = 4, 5, 6 respectively (for the inner density slope  $\gamma = 1$ ).

We now move to discuss the WSC for one–component n- $\gamma$  models: the obtained  $s_{\rm a}(n,\gamma)$  will mark a lower limit above which consistency (for the considered n and  $\gamma$ ) is guaranteed. Unfortunately, the WSC cannot be explored algebraically in the general case, because the resulting inequality (that for simplicity we do not report here) involves the solution of an equation of fifth degree for n=5, and the degree increases for increasing n. For n=4, instead, it is possible to treat the WSC analytically, since it reduces

to the discussion of a cubic equation (see C99). Of course, the critical values for the anisotropy radius can be easily obtained solving numerically inequality (6) in any specific case of interest, and the results are shown in Fig. 2 for n=4,5,6 with dashed lines: all one–component n- $\gamma$  models with the pair  $(s_a,\gamma)$  in the region above the dashed lines are consistent. Note how for increasing values of the external density slope n more and more radially anisotropic orbital distributions can be supported, thus confirming the indications provided by the NC.

Values of  $s_a$  nearer to the limits set by the DF are obtained by using the SSC. Inequality (5) evaluated for a generic pair  $(\gamma,n)$  results in a transcendental equation that must be studied numerically (as already done for n=4 in C99), and the black dots joined by the dotted lines in Fig. 2 represent the critical lower values of  $s_a$  for one–component  $\gamma$  models with  $\gamma=0,1,2$ , and n=4,5,6. As expected, the dotted lines are contained between the solid (NC) and the dashed (WSC) lines in each panel, and again they shift downward for increasing n.

Thus, from this preliminary investigation of one-component n- $\gamma$  models we conclude that for fixed  $\gamma$  an increase of n corresponds to a decrease of the minimum admissible value of  $s_a$ , i.e. steeper density distributions in the external regions can support more radial anisotropy.

# 3.2 Sufficient conditions for halo-dominated $(n-\gamma,\gamma_1)$ models

In order to proceed further with the preliminary discussion, we now apply the WSC to the  $n-\gamma$  component of a  $(n-\gamma,\gamma_1)$ model, extending to this class of systems some of the results obtained in C96 and C99 for two-component  $(\gamma_1, \gamma_2)$ models. In particular, the analytical study in C99 was restricted to some representative  $(\gamma_1, \gamma_2)$  models, namely a) isotropic two-component systems with inner slopes in the ranges  $1 \leq \gamma_1 < 3$ , and  $0 \leq \gamma_2 \leq \gamma_1$  (i.e. the  $\gamma_2$  component is shallower in the central regions); b) isotropic twocomponent (0,1) systems (i.e. the  $\gamma_2$  component is steeper in the central regions); and finally c) anisotropic  $\gamma_1$  profiles with  $1 \leq \gamma_1 < 3$  in the gravitational field of a dominant central black hole. Here, in order to obtain analytical results for the more general  $(n-\gamma,\gamma_1)$  models, we assume that the  $\gamma_1$  component (the "halo") dominates everywhere the gravitational field. Under this simplifying assumption, the following three results, corresponding to the points a), b), and c) above, will be proved analytically:

- (i) In the case of halo-dominated isotropic  $(n-\gamma,\gamma_1)$  models, with  $1 \leq \gamma < 3$ ,  $0 \leq \gamma_1 \leq \gamma$ , and n > 3, the centrally more peaked  $n-\gamma$  component is consistent, independently of the value  $\xi = r_c/r_1$  of its concentration relative to the centrally flatter  $\gamma_1$  halo. In the case of anisotropic  $(n-\gamma,\gamma_1)$  models, the determination of a minimum anisotropy radius for consistency as a function of  $n,\gamma,\gamma_1,\xi$  reduces to the solution of an algebraic equation of sixth degree (for generic n), which is solved numerically. In the particular case of halo-dominated (n-2,1) models, the application of the WSC shows that for  $\xi \leq (n-1)/2$  these models can be consistently assembled using radial orbits only.
- (ii) In the case of halo-dominated isotropic (n-0,1) models, the WSC shows that for  $\xi \leq (n+1)/2$  the n-0 density

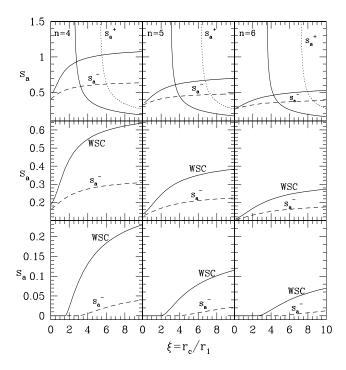


Figure 3. Minimum value of the anisotropy radius (normalized to the scale–length of the n- $\gamma$  component, i.e.  $s_{\rm a}=r_{\rm a}/r_{\rm c})$  as a function of the relative concentration  $\xi$ , for consistency of halo dominated (n- $\gamma$ ,1) models. The external density slope n increases as n=4,5, and 6 from left to right panels, while the internal density slope as  $\gamma=0,1$ , and 2 from top to bottom panels. Solid lines represent the limits derived from the WSC, while dashed lines are the  $s_{\rm a}^-$  derived from the DF. Note that for (n-0,1) models also the  $s_{\rm a}^+$  limits appear for  $\xi>\xi_{\rm c}$  (see Sections 3.2 and 4.3 for details).

distribution is consistent. For broader n-0 density distributions, the models can be consistent only in presence of some amount of radial anisotropy.

(iii) In the case of anisotropic n- $\gamma$  models with a dominant black hole at their center it is possible to determine analytically a lower limit  $r_{\rm a}(n,\gamma)$  for consistency, and this limit decreases for increasing n.

The proof of the first result, which is an extension of the study mentioned in point a), is conceptually straightforward but algebraically cumbersome, and only the main steps are reported in Appendix A (eq. [A3]). In particular, as this result holds also for n > 3, while the external logarithmic slope of the  $\gamma_1$  halo is 4, it means that a centrally steep density profile can be consistent in the gravitational field of a more massive (but centrally shallower) component, even when its external regions are less peaked. The situation is illustrated for some representative cases in Fig. 3 (bottom and middle panels), where all points above the solid lines correspond to consistent halo-dominated (n-1,1) and (n-2,1)models, and apparently the isotropic limit  $(s_a = \infty)$  is allowed for any choice of  $\xi$ ; the solid lines are obtained by solving numerically the corresponding WSC. A few additional trends are apparent. First, for a given central logarithmic density slope  $\gamma$  and for a given relative concentration  $\xi$ , an increase of n corresponds to a better and better ability to sustain radial anisotropy, and thus the trend found in onecomponent models is confirmed also in the two-component case. Second, at fixed n and  $\gamma$ , the minimum anisotropy radius for consistency increases for increasing  $\xi$ . This trend was already found in C96 and C99; in practice, in a fixed potential broader density distributions are less and less able to sustain radial anisotropy. Third, at fixed external slope n and relative concentration  $\xi$ , more centrally peaked systems are better able to support radial anisotropy. An additional comment concerns the specific case of (n-2,1) models (Fig. 3, bottom panels). In fact, it is apparent how in presence of a dominant  $\gamma_1 = 1$  halo the WSC limits flatten to zero for relative concentration less than some critical value  $\xi_c$ , and accordingly the model may be purely radially anisotropic. Remarkably, it is easy to show that the n-2 component can support purely radial orbits for relative concentrations  $\xi \leq \xi_c = (n-1)/2$  (see eq. [A4]), which are exactly the critical points in Fig. 3. Of course, this is just a sufficient condition, so we expect that the existence of a larger critical concentration for consistency in case of purely radial orbits will be revealed by direct inspection of the DF. A final comment is due. In fact, the adopted range of values for the internal density slopes  $\gamma > \gamma_1$  imply that the halo density distribution is centrally less peaked than the  $n-\gamma$ component. Therefore, for large but *finite* total halo mass, the integrated mass of the halo is subdominant with respect to the stellar one for vanishing r, and the assumption of a dominant halo breaks down at the very center. This means that in an asymptotic sense, the analysis presented in the previous Section should be applied at the center of these finite-halo mass models.

Result (ii) extends the study mentioned in point b) above, and it is proved in eq. (A5). The obtained limitation  $\xi \leq \xi_c = (n+1)/2$ , shown by the solid line in Fig. 4, suggests that the concentration of the  $\gamma = 0$  component must "adapt" to the dominant  $\gamma_1 = 1$  halo for phase–space consistency. Note that  $\xi_c$  increases for increasing n, i.e. a steeper external density profile can (partially) compensate for the effect of a central shallower density distribution. The appearence of the concentration limit  $\xi_c$  in the isotropic case manifests in the top panels of Fig. 3. In fact, as discussed in Section 2, in systems with positive isotropic functions (WSC or DF) only a lower limit for  $s_a$  exists, as in the case of halo dominated (n-1,1) and (n-2,1) models. In the present case, instead, when for increasing  $\xi$  the critical value  $\xi_c = 2.5$ is crossed (in the n = 4 panel), the additional condition  $s_a < s_a^+$  corresponding to the radial domain  $A_-$  appears as the vertical asymptote of the solid line, and the parameter space for consistency progressively reduces, shrinking to zero for the value of  $\xi$  where the two solid lines (obtained numerically) cross. A similar configuration repeats in the panels representing the n=5 and n=6 cases, where the consistency limits move, as expected, downward and rightward. Of course, these limits represent only a sufficient condition for the consistency, and when considering the DF in the limit  $\mu \to 0$  (see Section 4) we expect to determine larger critical values of  $\xi_c$ , and larger consistency regions in the  $(\xi, s_a)$ plane.

The result concerning the models with central black hole, related to point c) above, is proved as follows. As well known, for  $r_1 \to 0$  the potential of the  $\gamma_1 = 1$  model becomes that of a point mass, and from the first result proven in this

Section it follows that a black hole of any mass  $M_{\rm BH}$  can be consistently added at the center of a globally isotropic  $n\text{-}\gamma$  model, when  $1 \leq \gamma < 3$  and n > 3. For this reason in the following we restrict to this range of slopes  $\gamma$ , and accordingly the long-dashed curves in Fig. 2 interrupt for  $\gamma < 1$ . Having reduced the study to models with a positive isotropic DF, we only have to estimate a lower limit of  $r_{\rm a}$ . In Appendix A the WSC is applied to the anisotropic  $(n\text{-}\gamma, \text{BH})$  models with  $1 \leq \gamma < 3$ ; it can be discussed analytically in the special case of a dominant black hole, i.e. assuming in eq. (6)  $M_{\rm T} = M_{\rm BH}$  (and so  $\Psi_{\rm T} = GM_{\rm BH}/r$ ). As shown in eq. (A6), under these assumptions

$$s_{\rm a} \ge s_{\rm M} \sqrt{\frac{(3-\gamma)(\gamma-2) + s_{\rm M}(n-2)[(6-2\gamma) - (n-3)s_{\rm M}]}{n(n-1)s_{\rm M}^2 + 2n(\gamma-1)s_{\rm M} + \gamma(\gamma-1)}},$$
(23)

where  $s_{\rm M}=s_{\rm M}(n,\gamma)$  is obtained by solving an algebraic equation of fourth degree: the obtained limits are shown in Fig. 2 with the long-dashed lines, for n=4,5,6. For n=4 equation above coincide with that given in eq. (18) of C99, while asymptotic analysis proves that for  $n\to\infty$ 

$$s_{\rm M}(n,\gamma) = \frac{s_{\rm M0}(\gamma)}{n} + {\rm O}(n^{-2}),$$
 (24)

where  $s_{\text{M0}}(\gamma)$  is the larger real root of eq. (A9). We found that the substitution of eq. (24) in eq. (23) leads to estimates of the minimum  $s_{\text{a}}$  discrepant from the values obtained by the full formula by less than 50%, 33%, and 23% for n=4,5,6 respectively (for the inner density slope  $\gamma=1$ ). As in the other cases, an increase of the external density slope n makes it possible to sustain more radial orbits.

## 4 THE DF OF HALO-DOMINATED $(n-\gamma,\gamma_1)$ MODELS

It should be clear that the DF of two-component  $(n-\gamma,\gamma_1)$ models cannot be obtained analytically, except for very special combinations of the values of  $n, \gamma$ , and  $\gamma_1$ , as for example the (1,1) models discussed in C96 (that would be referred as (4-1,1) models in the present notation). However, the search is not hopeless. In fact, from C99 it is known that the halo dominated DF of two-component (1,0) and (0,1) galaxy models can be obtained in terms of elementary functions, and a simple argument shows that this is also the case of (2,1) and (2,0) models. This fact, the linearity of the OM inversion formula with respect to  $\rho$  in the non self-gravitating case (see eq. [2]), and finally the formula (18) for n integer, prove that also the DF of the halo dominated  $(n-\gamma,1)$  and  $(n-\gamma,0)$  models can be expressed in terms of elementary functions, for any integer  $n \geq 4$  and  $\gamma = 0, 1, 2$ . Note that, albeit their special nature, the study of halo-dominated models is useful because the formulae - expressible using elementary functions - can be studied very easily, making apparent the effects of the relative distribution of the investigated component and of the halo. In particular, in this Section we will determine the DF of the  $n-\gamma$  component of halo dominated  $(n-\gamma,1)$  models, and the exact phase-space constraints will be derived and compared with those obtained using the NC, WSC, and SSC in Section 3. We restrict to the  $\gamma_1 = 1$  case because the Hernquist

(1990) potential is the simplest in the class of  $\gamma$  models; furthermore, this choice allows us to investigate the consistency of models with central density slopes flatter ( $\gamma = 0$ ), equal ( $\gamma = 1$ ), and steeper ( $\gamma = 2$ ) than that of the halo. As a consequence, the results obtained for  $(n-\gamma,1)$  models should be representative of the whole situation.

With the normalization scales introduced at the beginning of Section 3, the relative potential of the Hernquist halo needed for the recovery of the DF is

$$\Psi(r) = \frac{\Psi_{\rm N}}{1+s} = \Psi_{\rm N}\tilde{\Psi}(s),\tag{25}$$

while from eq. (18)

$$\rho_n(r) = \rho_N \frac{\mu \xi^{n-3} (3-\gamma)(-1)^n}{4\pi \Gamma(n-3) s^{\gamma}} \frac{d^{n-4} (\xi+s)^{\gamma-4}}{d\xi^{n-4}}.$$
 (26)

As for the density and the potential, also for the DF it is useful to work with dimensionless functions, and we define  $f = f_{\rm N} \tilde{f}(\tilde{Q})$  with  $f_{\rm N} = \rho_{\rm N} \Psi_{\rm N}^{-3/2}$ , and  $0 \leq \tilde{Q} = Q/\Psi_{\rm N} \leq 1$ : note that, at variance with C99, the normalization quantities used here are those of the halo, consistently with the halo dominated nature of the present models. In other words, the dominant density distribution sets the natural scales. The easiest way to compute the DF is to change the integration variable from the total potential to the radius in the first of the identities in eq. (2). After normalization we obtain

$$f(Q) = \frac{f_{\rm N}}{\sqrt{8\pi^2}} \left(\frac{d\tilde{Q}}{d\nu}\right)^{-1} \frac{d\tilde{F}(\nu)}{d\nu}, \quad \nu = \nu(\tilde{Q}), \tag{27}$$

where

$$\tilde{F}(\nu) = -\int_{\nu}^{\infty} \frac{d\tilde{\varrho}_n}{ds} \frac{ds}{\sqrt{\tilde{\Psi}(\nu) - \tilde{\Psi}(s)}}$$

$$= \tilde{F}_i(\nu) + \frac{\tilde{F}_a(\nu)}{s_a^2}, \tag{28}$$

and from eq. (25)

$$\tilde{Q} = \frac{1}{1+\nu}, \quad \left(\frac{d\tilde{Q}}{d\nu}\right)^{-1} = -(1+\nu)^2, \quad 0 \le \nu \le \infty. \quad (29)$$

In the equations above, a negative sign appears in front of the integral (28) due to the monotonic decrease of the relative potential with increasing radius;  $\tilde{\varrho}_n$  is the normalized augmented density associated with eq. (26), while  $s_a = r_a/r_1$ is the normalized anisotropy radius; finally, the subscripts of the functions F refer to the isotropic and anisotropic parts of the DF, respectively. It is now evident how in halo dominated  $(n-\gamma,\gamma_1)$  models the external slope parameter appears in the density  $\tilde{\varrho}_n$  only, so that the DF of the n- $\gamma$  component can be obtained by repeated differentiation with respect to  $\xi$  of the simpler DF of the halo dominated  $(\gamma, \gamma_1)$  model. In the following, we will also discuss black hole dominated  $(n-\gamma,BH)$  models: then, we will adopt as natural normalization scales the black hole mass  $M_{\rm BH}$  and the scale-length  $r_{\rm c}$ of the n- $\gamma$  component; moreover,  $0 \leq \tilde{Q} \leq \infty$ , since in this case  $\tilde{\Psi} = 1/s$ , so that in eq. (29)  $\tilde{Q} = 1/\nu$ .

It is not difficult to show that, for generic values of  $\gamma$ , the integral (28) can be expressed as a combination of hypergeometric  ${}_2F_1$  functions when the halo is a  $\gamma_1 = 0$ , or 1 model, or a black hole. However, the resulting expressions are not more illuminating than the integral itself, so that we do not report them here. Instead, we prefer to show simple asymptotic expansions relative to a couple of interesting

situations. The first concerns the behaviour of the DF of  $(n-\gamma, BH)$  models for  $\tilde{Q} \to \infty$ , for which the leading term of the expansion (normalized to  $f_N/\sqrt{8}\pi^2$ ) is

$$\tilde{f}(\tilde{Q}) \sim \gamma \left(\gamma - \frac{1}{2}\right) \tilde{Q}^{\gamma - 3/2}$$
: (30)

thus, the slope  $\gamma=3/2$  marks the different behaviour of the models. We note also that f<0 for  $\gamma<1/2$  and the model is inconsistent (Tremaine et al. 1994); furthermore, we note how in the leading term above the function  $\tilde{F}_{\rm a}$  is producing no contribution. The other case of interest is the behaviour of the DF of isotropic n- $\gamma$  models for  $\tilde{Q}\to 0$ . We recall that this case is very general, as it applies to self-gravitating n- $\gamma$  models but also to n- $\gamma$  models in generic halos of finite total mass, because in all systems  $\Psi_{\rm T}\sim GM_{\rm T}/s$  for  $s\to\infty$ . In this case we found

$$\tilde{f}(\tilde{Q}) \sim n \left(n - \frac{1}{2}\right) \tilde{Q}^{n-3/2},$$
(31)

an expression (obviously) formally identical to eq. (30). Finally, we notice that the asymptotic expansion for  $r \to \infty$  of the velocity dispersion of isotropic n- $\gamma$  models (both single component and embedded in dark matter halos of finite total mass) is  $\sigma_{\rm r}^2 \sim 1/(n+1)s$ , normalized to  $GM_{\rm T}/r_{\rm c}$ , so that for  $r \to \infty \ \rho/\sigma_{\rm r}^3 \sim (n+1)^{-3/2} s^{3/2-n}$ , in accordance with the comment in Footnote 1.

### 4.1 The halo dominated (n-2,1) Model

Following the preliminary discussion, here we derive the explicit expression for the DF of the n-2 model with an arbitrary degree of OM orbital anisotropy, in the gravitational field of a dominant Hernquist halo. After partial fraction decomposition of eq. (28), the isotropic and anisotropic components of the DF are

$$\tilde{F}_{i}(\nu) = \frac{(-1)^{n} \mu \sqrt{1+\nu} \, \xi^{n-3}}{2\pi (n-4)!} \, \frac{d^{n-4}}{d\xi^{n-4}} \left( \frac{G_3 + G_3^0}{\xi^2} + \frac{G_2 - G_2^0}{\xi^3} \right), \tag{32}$$

and

$$\tilde{F}_{a}(\nu) = \frac{(-1)^{n} \mu \sqrt{1 + \nu} \, \xi^{n-3}}{2\pi (n-4)!} \frac{d^{n-4} G_{3}}{d\xi^{n-4}}$$

$$= \frac{\mu \sqrt{1 + \nu} (n-2)! \, \xi^{n-3} \, G_{n-1}}{4\pi (n-4)!},$$
(33)

respectively, where for  $k \geq 2$  we define

$$G_k(\xi,\nu) \equiv \int_{\nu}^{\infty} \sqrt{\frac{s+1}{s-\nu}} \frac{ds}{(\xi+s)^k}, \qquad G_k^0(\nu) \equiv G_k(0,\nu).$$
(34)

For  $\xi = 1$  the function  $G_k$  assume a very simple form:

$$G_k(1,\nu) = \frac{\sqrt{\pi} \Gamma(k-1)}{\Gamma(k-1/2)(1+\nu)^{k-1}},$$
(35)

while for  $\xi \neq 1$  the formula

$$G_{k+1}(\xi,\nu) = -\frac{1}{k} \frac{dG_k(\xi,\nu)}{d\xi} = \frac{(-1)^{k-1}}{k!} \frac{d^{k-1}G_2(\xi,\nu)}{d\xi^{k-1}}$$
(36)

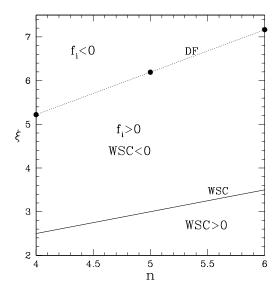
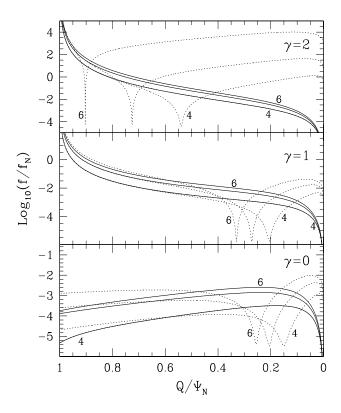


Figure 4. Upper limits for consistency on the concentration parameter  $\xi = r_{\rm c}/r_1$  of the fully isotropic halo-dominated (n-0,1) model, as a function of the external density slope n. The solid line is the limit derived from the WSC (Section 3.2), while the dotted line is the true limit obtained from the DF (Section 4.3).

holds, with

$$G_{2}(\xi,\nu) = \frac{1}{\xi + \nu} + \frac{1 + \nu}{(\xi + \nu)^{3/2}} \begin{cases} \frac{1}{\sqrt{1 - \xi}} \arctan\sqrt{\frac{1 - \xi}{\xi + \nu}}, & (0 \le \xi < 1), \\ \frac{1}{\sqrt{\xi - 1}} \arctan\sqrt{\frac{\xi - 1}{\xi + \nu}}, & (\xi > 1). \end{cases}$$
(37)

Note that the second expression in eq. (33) has been obtained from the relation (36). From the derived formulae we determined the true anisotropy limit for the (n-2,1) models. We found that  $f_i > 0$  for all the explored values of n, i.e. the isotropic n-2 model in a dominant Hernquist halo is consistent independently of the halo scale-length, in accordance with the result in point 1) of Section 3.2, obtained with the WSC. Therefore the set  $A_{+}$  in phase–space coincides with the whole accessible phase-space, and only the anisotropy limit  $s_{\rm a}^-$  exists. In Fig. 5 (top panel) we show the isotropic (solid) and strongly anisotropic (i.e., near to the consistency limit) DFs for n = (4,5,6) and  $\xi = 5$ . Note how the isotropic DFs are very similar, and monotonically decreasing. Instead, in the anisotropic cases the depression leading to inconsistency is apparent, clearly showing how phase–space inconsistency is always set outside the center. This feature is qualitatively similar to the others explored OM systems (e.g., see Fig. 2 in Ciotti & Lanzoni 1997, Figs. 2 and 3 in C99, Fig. 3 in Ciotti, Morganti & de Zeeuw 2008); in addition, the systematic shift of the DF depression towards high Q values for increasing n is also apparent: an argument supporting this phenomenon is given in Section 2.1.1. We notice that the cuspy dips shown by the DFs for values of  $s_a$ near the consistency limit could be the source of kinetic instabilities, whose investigation is of course well beyond the framework of this paper. In any case, it is almost certain that any system would develop radial orbit instability for



**Figure 5.** From top to bottom: the dimensionless DF for the halo dominated (n-2,1), (n-1,1), and (n-0,1) models, as a function of  $\tilde{Q}$ . The solid lines represent the isotropic DFs, while the dotted lines are the anisotropic DFs, with  $s_a$  approaching the critical value for consistency. In all cases,  $\xi = 5$ .

values of the anisotropy radius larger than the consistency limit (e.g., see the N-body experiments discussed in Nipoti, Londrillo & Ciotti 2002): therefore, the critical DFs in Fig. 5 describe equilibrium unstable systems.

The trend of the anisotropy limit  $s_a^-$  for different values of n and increasing  $\xi$  is shown in Fig. 3 (bottom panel) with the dashed lines. First, for fixed n and increasing  $\xi$ ,  $s_a^-$  increases: in practice, for a given halo, a broader stellar density distribution is less and less able to sustain radial anisotropy. Second, at fixed  $\mathcal{E}$  a steeper external density slope (i.e. larger n) corresponds to higher amount of admissible radial anisotropy, thus showing that not only the inner density slope, but also the external density profile is important for phase–space consistency. As expected, the true limitation on  $s_a^-$  is less stringent than the corresponding limit derived from the WSC, and the dashed line is everywhere below the solid line. In particular, while from the WSC the critical concentrations  $\xi_c$  in order to have a purely radial model are 1.5, 2, and 2.5 (for n = 4, 5, and 6), from the DF we obtain  $\xi_c \simeq 2.8, 3.7, \text{ and } 4.5.$ 

It is also possible to determine the DF of (n-2,BH) models in presence of a dominant central black hole. The resulting formulae are identical to eqs. (32)-(33), where the quantity  $\sqrt{1+\nu}$  at numerator is replaced by  $\sqrt{\nu}$  and the G functions are replaced by the corresponding  $G_{\bullet}$  functions of

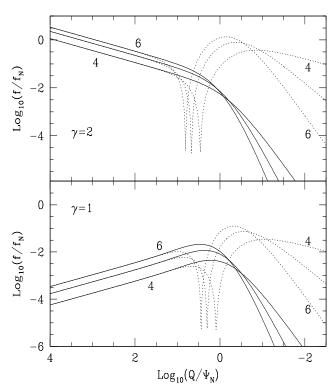


Figure 6. Dimensionless DF for the black hole dominated (n-2,1) and (n-1,1) models, as a function of the relative energy  $\tilde{Q}$ , for n=4,5, and 6. Normalization scales are the mass of the black hole and the scale–length of the  $n-\gamma$  component. Solid lines represent the isotropic DFs, while dotted lines the anisotropic DFs, with  $s_a$  approaching the critical value for consistency.

same index, defined for  $k \geq 2$  as

$$G_{\bullet k}(\xi, \nu) \equiv \int_{\nu}^{\infty} \sqrt{\frac{s}{s - \nu}} \frac{ds}{(\xi + s)^k},\tag{38}$$

and

$$G_{\bullet k}^{0}(\nu) \equiv G_{\bullet k}(0, \nu) = \frac{\sqrt{\pi} \Gamma(k-1)}{\Gamma(k-1/2)\nu^{k-1}}.$$
(39)

For  $\xi > 0$  the formula

$$G_{\bullet k+1}(\xi,\nu) = -\frac{1}{k} \frac{dG_{\bullet k}(\xi,\nu)}{d\xi} = \frac{(-1)^{k-1}}{k!} \frac{d^{k-1}G_{\bullet 2}(\xi,\nu)}{d\xi^{k-1}}$$
(40)

holds, where

$$G_{\bullet 2}(\xi, \nu) = \frac{1}{\xi + \nu} + \frac{\nu}{(\xi + \nu)^{3/2} \sqrt{\xi}} \operatorname{arctanh} \sqrt{\frac{\xi}{\xi + \nu}}.$$
 (41)

Note that after performing the required differentiations one must set  $\xi=1$ . In Fig. 6 (upper panel) the obtained DFs are shown in the isotropic (solid lines) and strongly anisotropic (dotted lines) cases. Again, inconsistency due to OM anisotropy affects the DF at intermediate energies. The true anisotropy limits derived from the DF are given by solid squares in Fig. 2. Finally, note also the characteristic log-log linear trend of the DF for very high values of Q. This trend

is easily explained by considering the asymptotic expansion given in eq. (30).

### 4.2 The halo dominated (n-1,1) Model

We now derive the explicit DF for the family of halo dominated (n-1,1) models, so that with this class of models we can study the effect of the external logarithmic slope when the two density profiles have the same inner slope. Of course, the (4-1,1) models are the halo dominated of (1,1) models discussed in C96.

Integration of eq. (28) reveals that the functions involved in the expression of the DF are the same as for the (n-2,1) models. In particular,

$$\tilde{F}_{\rm i}(\nu) = \frac{(-1)^n \mu \sqrt{1 + \nu} \, \xi^{n-3}}{2\pi (n-4)!} \frac{d^{n-4}}{d\xi^{n-4}} \left( \frac{G_2^0 - G_2}{\xi^3} - \frac{2G_3}{\xi^2} - \frac{3G_4}{\xi} \right),\tag{42}$$

and

$$\tilde{F}_{a}(\nu) = \frac{(-1)^{n} \mu \sqrt{1+\nu} \, \xi^{n-3}}{2\pi (n-4)!} \, \frac{d^{n-4} (2G_3 - 3\xi G_4)}{d\xi^{n-4}}.$$
 (43)

In Fig. 5 (middle panel), the DF in the isotropic and strongly anisotropic cases is shown, for n = 4, 5, 6. The behaviour is qualitatively similar to that of (n-2,1) models, i.e. while the isotropic systems display a monotonically decreasing DF, in the anisotropic case (when  $s_{\rm a}^-$  approaches the consistency limit) the DF has a significant depression, that moves inwards for increasing n. In Fig. 3 (middle row) we show the minimum value of the anisotropy radius normalized to  $r_c$  as derived from the DF (dashed lines), and from the WSC. Again, in accordance with the preliminary study of Section 3.2, we found that  $f_i > 0$  independently of the relative concentration value  $\xi$  and of the external slope n, so that only the limit  $s_a^-$  exists. All the trends exhibited by the (n-2,1) models are confirmed: in particular,  $s_a^-$  increases with  $\xi$  for fixed n, while it decreases at fixed  $\xi$  for increasing n. Note that the maximum radial anisotropy admissible for given  $\xi$  and n is smaller than for (n-2,1) models, as expected from the shallower central profile of n-1 models. Finally, at variance with the (n-2,1) models (and in agreement with the expectations of the preliminary analysis) no purely radial orbital configurations can be supported, independently of the value of the concentration  $\xi$ .

As for (n-2,BH) models, also in the case of the black hole dominated (n-1,BH) models the functions  $\tilde{F}_i$  and  $\tilde{F}_a$  are formally identical to those in eqs. (42)-(43), with each G function replaced by the corresponding  $G_{\bullet}$  function, and with the substitution  $\sqrt{1+\nu} \to \sqrt{\nu}$ ; again, it is necessary to set  $\xi=1$  after performing the required differentiations. While the true limits on the anisotropy radius are plotted in Fig. 2 with the solid squares, the obtained DFs are shown in the isotropic (solid) and strongly anisotropic (dotted) cases in the bottom panel of Fig. 6; not unexpectedly, the inconsistency due to anisotropy manifests itself at intermediate energies. Finally, the behaviour of the DF for very high values of Q is in accordance with the asymptotic expansion of the DF in eq. (30).

## 4.3 The halo dominated (n-0,1) Model

This case is expected to be the more complicated, because from C99 it is known that the (0,1) model presents a peculiar behaviour: in practice, there exists a range of  $\xi$  where anisotropic models can be consistent when instead isotropic models are not, and this is due to the fact that  $f_i$  becomes negative over the non empty set  $A_-$ , so that two limits on  $s_a$  must be considered. Note that the discussion of the WSC in the case of (n-0,1) models in Section 3.2 already showed a similar behaviour.

As in the other cases, the integration of eq. (28) can be done by using the  $G_k$  functions only:

$$\tilde{F}_{i}(\nu) = \frac{(-1)^{n} 3\mu \sqrt{1+\nu} \, \xi^{n-3}}{\pi (n-4)!} \frac{d^{n-4} G_{5}}{d\xi^{n-4}} 
= \binom{n}{4} \frac{3\mu \sqrt{1+\nu} \, \xi^{n-3} G_{n+1}}{\pi},$$
(44)

$$\tilde{F}_{a}(\nu) = \frac{(-1)^{n} 3\mu \sqrt{1+\nu} \, \xi^{n-3}}{2\pi (n-4)!} \frac{d^{n-4} (2\xi^{2} G_{5} - 3\xi G_{4} + G_{3})}{d\xi^{n-4}},\tag{45}$$

where the second expression for  $F_i$  is obtained from the relation (36) of the  $G_k$  functions. Motivated by the remarks above, we start to study the sign of  $f_i$ , in order to determine the condition for the existence of the sets  $A_{+}$  and  $A_{-}$ . Indeed, we found that for  $\xi \lesssim 5.233$  (in the n=4 case, see C99),  $\xi \lesssim 6.192$  (for n = 5), and  $\xi \lesssim 7.166$  (for n = 6),  $f_i$  is positive everywhere over the accessible phase-space, a situation which is graphically represented with the dotted lines in Fig. 4. It follows that for sufficiently concentrated models only the anisotropy limit  $s_{\rm a}^-$  exists, and in Fig. 5 (bottom panel, solid lines) the isotropic DF is shown for (n-0,1) models with  $\xi = 5$  and n = (4, 5, 6): note how, at variance with the other cases, the DF of (n-0,1) models decreases for increasing Q. The trend of  $s_a^-(\xi)$  is shown in Fig. 3 (top panels, dashed lines): as for the models previously discussed, the  $s_a^$ curve is similar (but displaced) with respect to that derived from the WSC. It is apparent how the  $s_{\rm a}^-$  line lies above those of n-1 and n-2 models, as expected from the shallower density profile of n-0 models; moreover, we note how the minimum admissible values for  $s_a^-$  decrease for increasing n, as in the other cases. In Fig. 5 the DFs for  $s_a$  near the consistency limit  $s_{\rm a}^-$  are shown with dotted lines for models having  $\xi = 5$ , and as in the previous  $\gamma = 1$  and  $\gamma = 2$ models, inconsistency appears at intermediate values of Q.

For values of  $\xi$  larger than the critical values of  $\xi_c$  reported above, the set  $A_-$  is not empty, because the isotropic component of the DF becomes negative at high relative energies. In fact, at variance with the (n-2,1) and (n-1,1) models, the DF of the n-0 model converges to a finite limit (that can be easily calculated analytically from eq. [44]) for  $\tilde{Q}=1$ ; when increasing  $\xi=r_0/r_1$ , the value  $\tilde{f}(1)$  monotonically decreases, till it becomes negative for  $\xi$  greater than  $\xi_c$ . A similar behavior was found in the numerical investigation of consistency of King (1972) and quasi-isothermal halos added to a de Vaucouleurs (1948) density distribution (see CP92). Thus, while the effects of OM radial anisotropy appear to affect the DF at intermediate energies, the inconsistency of isotropic models embedded in a peaked halo seems

to characterize the DF at very high (relative) energies. According to the discussion of Section 2, since the function  $f_a$  is positive on  $A_-$ , the upper bound  $s_a^+$  can be determined: the appearence of this new value is manifested by the dotted lines in Fig. 3, with the vertical asymptote corresponding to  $\xi_c$ . Then, for  $\xi$  greater than the critical limit, a range of concentrations exists where an anisotropy radius  $r_a^- \leq r_a \leq r_a^+$  corresponds to consistent models; finally, for  $\xi$  larger than the value where the dotted  $(s_a^+)$  and dashed  $(s_a^-)$  lines cross each other,  $s_a^- > s_a^+$ , and the models become inconsistent. Summarizing, consistent models correspond to points placed above the  $s_a^-$  line and on the left of the  $s_a^+$  line.

In the case of a central dominant black hole, the same comments as those for (n-2,BH) and (n-1,BH) models apply, and the functions  $\tilde{F}_{\rm i}$  and  $\tilde{F}_{\rm a}$  are obtained accordingly. Of course, the isotropic model is inconsistent, independently of the values of n, because the model with black hole would correspond to the formal limit  $\xi \to \infty$  in (n-0,1) models, which is already excluded by the previous discussion. What happens when considering the effect of anisotropy? Is there any compensating effect? A numerical inspection shows that the anisotropic part of the DF is negative on  $A_-$ , so that not even orbital anisotropy can make the models consistent. Again, this result was expected from the study of (n-0,1) models, due to the crossing of the  $s_{\rm a}^-$  and  $s_{\rm a}^+$  critical lines at finite values of  $\xi$ .

### 5 DISCUSSION AND CONCLUSIONS

In this paper, in a natural extension of previous investigations (CP92, C96, C99), we focused on the importance of the external density logarithmic slope on the determination of the phase–space consistency of one and two–component stellar systems with OM orbital anisotropy. In particular, the considered  $(n-\gamma,\gamma_1)$  models generalize  $(\gamma_1,\gamma_2)$  models, as the  $n-\gamma$  density component is characterized by logarithmic slope n instead of 4 outside the core radius, while in the inner regions the logarithmic density slope is  $\gamma$ . The main results can be summarized as follows:

- (i) It is shown that, for n integer, several structural and dynamical properties of the n- $\gamma$  models can be obtained by differentiation, with respect to the scale–length, of the corresponding formulae valid for the standard  $\gamma$  models. For example, it is shown how to construct explicit solutions of the Jeans equations for the class of two–component anisotropic  $(n_1$ - $\gamma_1, n_2$ - $\gamma_2)$  models once the solution is known for  $(\gamma_1, \gamma_2)$  models.
- (ii) In one-component n- $\gamma$  models, a lower limit for the anisotropy radius, so that smaller values certainly produce inconsistent models, is analytically derived following the technique introduced in CP92. It is found that for  $0 \le \gamma < 2$  this minimum anisotropy radius is strictly positive, but it decreases by increasing n, i.e. a larger amount of radial anisotropy can be supported by externally steeper density profiles. For  $2 \le \gamma < 3$  instead the necessary condition for consistency is satisfied  $\forall s_{\rm a} > 0$ , independently of the value of  $\gamma$  and n. The minimum anisotropy radius so that larger values correspond to consistent n- $\gamma$  models is then determined by using the strong and weak sufficient conditions for model consistency derived in CP92. As for the necessary condition,

we find that the minimum value of the anisotropy radius decreases for increasing  $\gamma$  and fixed n, and for increasing n and fixed  $\gamma$ .

- (iii) A similar analysis is then performed for twocomponent  $(n-\gamma,\gamma_1)$  systems, in order to extend the study of C99. For simplicity we restrict to halo dominated models, i.e. we take into account only the gravitational field of the  $\gamma_1$  halo. In particular, we show that in the isotropic case, when  $1 \le \gamma < 3$  and  $0 \le \gamma_1 \le \gamma$  (i.e., the halo density is centrally less peaked than the stellar component), the DF of the n- $\gamma$  component is nowhere negative, independently of the mass and concentration of the  $\gamma_1$  halo. This is true even when in the external parts the  $n\text{-}\gamma$  component is less peaked (3 < n < 4) than the  $\gamma_1$  component. As a special application of this result, it follows that a black hole of any mass can be consistently added at the center of a globally isotropic  $n-\gamma$  model, when  $1 < \gamma < 3$ . Moreover, in the case of (n-0.1)models, where instead the halo is centrally steeper than the stellar component, the sufficient condition applied to the n-0 density distribution reveals the existence of an upper limit  $\xi < (n+1)/2$  of the relative concentration  $\xi = r_0/r_1$ for model consistency in the isotropic case. Finally, in the case of anisotropic  $n-\gamma$  models with a dominant black hole at their center, we determined analytically a lower limit of the critical anisotropy radius for consistency as a function of n and  $\gamma$ ; this value decreases for increasing  $\gamma$  and/or n.
- (iv) The analytic expression for the DF of OM anisotropic halo dominated  $(n-\gamma,1)$  models, and  $(n-\gamma,\mathrm{BH})$  models with a dominant central BH is recovered in terms of elementary functions in the special cases when  $\gamma=(0,1,2)$ . It is found that, while for  $\gamma=1,2$  the isotropic DF is positive independently of the model concentration, the  $\gamma=0$  component becomes inconsistent when the halo is sufficiently concentrated, even in the isotropic case. In addition, the trend of the minimum value of the anisotropy radius as a function of the halo concentration confirms that steeper density profiles in the external region are consistent with a larger amount of radial anisotropy.

In conclusion, the explored family of models provide a direct indication that the density slope in the external regions of stellar systems can be important in determining the admissible radial anisotropy, and this in addition to the well known relevance of the central density slope. A quantification of this argument is embodied in a necessary inequality for model consistency, that we derived by expressing a previous finding (CP92) in terms of the logarithmic density slope. The obtained result holds for all consistent OM anisotropic systems, and relates the logarithmic density slope and the OM anisotropy indicator at each radius, in a way formally identical to the "cusp slope-central anisotropy" theorem by AE06, which is known to apply at the center of stellar systems with generic anisotropy distribution, and everywhere in constant anisotropy systems.

#### ACKNOWLEDGMENTS

We wish to thank the anonymous Referee for helpful suggestions that greatly improved the presentation of the paper.

# APPENDIX A: CONSISTENCY REQUIREMENTS

### A1 The NC for one-component n- $\gamma$ models

Simple algebra shows that the NC applied to anisotropic n- $\gamma$  models can be written as

$$s_{\mathbf{a}}^2 \ge \frac{2 - \gamma - (n - 2)s}{\gamma + ns} s^2, \quad 0 \le s \le \infty. \tag{A1}$$

For  $\gamma \geq 2$  and  $n \geq 2$  the r.h.s. is everywhere negative, so that inequality (A1) is trivially satisfied for  $s_a \geq 0$ . Instead, for  $0 \leq \gamma < 2$  the parameter  $s_a$  must be larger than the maximum of the expression of the r.h.s., which is reached at

$$s_{\rm M}(n,\gamma) = \frac{n - (2n-3)\gamma + \sqrt{(n-\gamma)[n+(4n-9)\gamma]}}{2n(n-2)},$$
 (A2)

that after substitution in eq. (A1) gives eq. (21). Of course, for n=4 eq. (A2) in C99 is reobtained.

### A2 The WSC for halo-dominated $(n-\gamma,\gamma_1)$ models

Here we apply the WSC to the n- $\gamma$  component of globally isotropic, halo-dominated (n- $\gamma$ , $\gamma_1)$  models, where  $1 \leq \gamma < 3$ ,  $0 \leq \gamma_1 \leq \gamma$ , and n > 3. Under the assumption of a dominant halo, eq. (6) reduces to investigate the positivity of an expression which factorizes in a strictly positive function and in an algebraic factor that after the natural substitutions  $\gamma = 1 + \epsilon$  and  $\gamma_1 = \gamma - \epsilon_1$  (with  $0 \leq \epsilon < 2$  and  $0 \leq \epsilon_1 \leq \gamma$ ) becomes

$$n(n-1)s^{3} + n[n+1-\epsilon+\epsilon_{1}+2\xi\epsilon]s^{2}$$

$$+\xi\{[(n+1)(2+\epsilon+\epsilon_{1})+\epsilon\epsilon_{1}-\epsilon^{2}]+\xi\epsilon\gamma\}s + \xi^{2}\gamma(2+\epsilon_{1}),$$
(A3)

whose positivity  $\forall (s,\xi) \geq 0$  is easily proved. Therefore the WSC is verified for any value of the concentration parameter  $\xi$ . Note that the variables  $\xi$  and s adopted here correspond to  $1/\xi$  and  $s/\xi$  respectively in eq. (A13) of C99, due to the different normalization length.

Being the WSC of the isotropic models satisfied, the existence of a critical anisotropy radius  $s_{\rm a}^-$  for consistency depends on the sign of the anisotropic part of the WSC, as discussed in Section 2.2. In particular, the positivity of the anisotropic WSC for (n-2,1) models reads

$$s(n-3) + n - 1 - 2\xi \ge 0, \quad 0 \le s \le \infty,$$
 (A4)

and thus shows the existence of a critical value  $\xi_{\rm c}=(n-1)/2$  of the concentration parameter, marking an upper limit on the values of  $\xi$  for which  $s_{\rm a}^-=0$ , i.e. purely radial orbital distributions are allowed.

The discussion of the WSC for globally isotropic n-0 models in a dominant  $\gamma=1$  halo is simple, reducing to the request that

$$s(n-1) + n + 1 - 2\xi \ge 0, \quad 0 \le s \le \infty,$$
 (A5)

which is satisfied for  $\xi \leq \xi_c = (n+1)/2$ . For n=4 we reobtain the result of C99.

In the case of central dominant BH, we assume in eq. (6)  $M_{\rm T}=M_{\rm BH}$ , and from the previous discussion we restrict to  $n\text{-}\gamma$  models with  $1\leq\gamma<3$ . The WSC then requires that

$$s_{\rm a}^2 \ge s^2 \frac{(3-\gamma)(\gamma-2) + 2(n-2)(3-\gamma)s - (n-2)(n-3)s^2}{n(n-1)s^2 + 2n(\gamma-1)s + \gamma(\gamma-1)}.$$

(A6)

After the differentiation of the r.h.s. and the successive study of a quartic equation, it can be proved that for  $s \ge 0$  eq. (A6) admits only one maximum, located at  $s_{\rm M} = s_{\rm M}(n,\gamma) \ge 0$ . The general expression for  $s_{\rm M}(n,\gamma)$  is not reported here, but it was used to produce the long-dashed lines in Fig. 2. In any case,  $s_{\rm M}(n,3) = 0$ ,

$$s_{\mathcal{M}}(n,\gamma) = \begin{cases} \frac{2}{n-3}, & \gamma = 1, \\ \frac{\sqrt[3]{s_0}}{3n(n-1)(n-3)} - \frac{2(n-4)}{3(n-1)(n-3)} \\ + \frac{4(n^3 + n^2 - 20n + 27)}{3(n-1)(n-3)\sqrt[3]{s_0}}, & \gamma = 2, \end{cases}$$
(A7)

where

$$s_0 = n^2 \left[ 73n^4 - 660n^3 + 2262n^2 - 3484n + 2025 + 9\sqrt{\frac{(5n-9)(13n^2 - 59n + 64)(n-1)^3(n-3)^3}{n}} \right], (A8)$$

and for n=4 and  $\gamma=1,2,3$  the values given in Table 1 of C99 are reobtained. We finally report the reduced asymptotic fourth-order equation needed to determine  $s_{\rm M}(n,\gamma)$  in the limit  $n\to\infty$ : remarkably, after the scaling s=y/n and the successive limit  $n\to\infty$ , one obtains

$$y^{4} + 2(2\gamma - 3)y^{3} + 6(\gamma - 1)(\gamma - 2)y^{2}$$

$$+ 2(\gamma - 3)(\gamma - 1)(2\gamma - 1)y + (\gamma - 3)(\gamma - 2)(\gamma - 1)\gamma = 0.$$
(A9)

# APPENDIX B: THE VELOCITY DISPERSIONS AND THE VIRIAL QUANTITIES FOR $(n_1-\gamma_1,n_2-\gamma_2)$ MODELS

Here we present an easy way to express analytically the main dynamical quantities of the two–component OM anisotropic  $(n_1-\gamma_1,n_2-\gamma_2)$  models for generic  $\gamma_1$  and  $\gamma_2$ , and  $n_1$  and  $n_2$  integer  $\geq 4$ . The method is based on the evaluation of the similar quantities for the two–components  $(\gamma_1,\gamma_2)$  models, and then on repeated differentiation with respect to the scale-lengths.

We start by considering the radial component  $\sigma_{\rm r}^2$  of the velocity dispersion  $\sigma^2 = \sigma_{\rm r}^2 + \sigma_{\rm t}^2$  of a system with a density component  $\rho$ , which in the OM parameterization can be written as

$$\rho(r)\sigma_{\rm r}^2(r) = \frac{A(r) + r_{\rm a}^2 I(r)}{r^2 + r_{\rm a}^2}, \tag{B1}$$

where

$$A(r) = G \int_{r}^{\infty} \rho(r) M_{\rm T}(r) dr, \quad I(r) = G \int_{r}^{\infty} \frac{\rho(r) M_{\rm T}(r)}{r^2} dr,$$
(B2)

(Binney & Mamon 1982), and  $M_{\rm T}(r)$  is the total mass within r. Once  $\sigma_{\rm r}^2$  is known, the tangential velocity dispersion is obtained from eq. (8).

As the method is general, we focus without loss of generality on the component "1" of a two-component model, for which the two functions I and A are given by the sum  $I_1 = I_{11} + I_{12}$  and  $A_1 = A_{11} + A_{12}$ , due to the linearity

of mass in eqs. (B2), and where the meaning of the subscript indices is apparent. Other quantities of interest in applications are the global energies entering the scalar virial theorem, and for the component 1 the scalar virial theorem reads  $2K_1 = |W_{11}| + |W_{12}|$ , where  $W_{11} = -4\pi G \int r \rho_1 M_1 dr$  is the contribution due to the self–interaction, and  $W_{12} = -4\pi G \int r \rho_1 M_2 dr$  is the interaction energy with the "halo" (e.g., Ciotti 2000).

The basic idea is to compute the integrals for the generic pair  $(\rho_1, M_2)$  relative to standard two–component  $(\gamma_1, \gamma_2)$  models with different scale–lengths  $r_{c1}$  and  $r_{c2}$ , to perform the required differentiations as prescribed by eqs. (18) and (19), and finally (in the case of self–interactions) to set the two scale–lengths and the two slopes to the same value. From eqs. (18) and (19) it follows

$$A_{12}(r) = G \frac{r_{c1}^{n_1 - 3} r_{c2}^{n_2 - 3} (-1)^{n_1 + n_2}}{\Gamma(n_1 - 3)\Gamma(n_2 - 3)}$$

$$\frac{d^{n_1 - 4}}{dr_{c1}^{n_1 - 4}} \frac{d^{n_2 - 4}}{dr_{c2}^{n_2 - 4}} \int_{r}^{\infty} \frac{\rho_{\gamma_1}(r, r_{c1}) M_{\gamma_2}(r, r_{c2})}{r_{c1} r_{c2}} dr, \text{ (B3)}$$

$$I_{12}(r) = G \frac{r_{c1}^{n_1 - 3} r_{c2}^{n_2 - 3} (-1)^{n_1 + n_2}}{\Gamma(n_1 - 3)\Gamma(n_2 - 3)}$$

$$\frac{d^{n_1 - 4}}{dr_{c1}^{n_1 - 4}} \frac{d^{n_2 - 4}}{dr_{c2}^{n_2 - 4}} \int_{r}^{\infty} \frac{\rho_{\gamma_1}(r, r_{c1}) M_{\gamma_2}(r, r_{c2})}{r_{c1} r_{c2} r^2} dr, \text{ (B4)}$$

$$W_{12}(r) = -4\pi G \frac{r_{c1}^{n_1 - 3} r_{c2}^{n_2 - 3} (-1)^{n_1 + n_2}}{\Gamma(n_1 - 3)\Gamma(n_2 - 3)}$$

$$\frac{d^{n_1 - 4}}{dr_{c1}^{n_1 - 4}} \frac{d^{n_2 - 4}}{dr_{c2}^{n_2 - 4}} \int_{0}^{\infty} \frac{\rho_{\gamma_1}(r, r_{c1}) M_{\gamma_2}(r, r_{c2})}{r_{c1} r_{c2}} r dr; \text{(B5)}$$

for generic values of  $\gamma_1$  and  $\gamma_2$  the integrals above involve hypergeometric  ${}_2F_1$  functions, while for integer values of  $\gamma_1$  and  $\gamma_2$  the resulting formulae can be expressed in terms of elementary functions (e.g., see C96 and C99 for (1,0) and (1,1) models; Ciotti et al. 1996 for (2,1) and (2,2) models). Even simpler expressions can be obtained without difficulty for to the halo dominated (n-0,1), (n-1,1), and (n-2,1) models, by adopting as normalization constants the physical scales  $M_1$  and  $r_1$  of the  $\gamma=1$  dominant component, and by fixing  $n_2=4,\,r_{\text{c2}}=r_1,\,n_1=n,\,\xi\equiv r_{\text{c1}}/r_1,\,s\equiv r/r_1,\,\mu\equiv M/M_1$  in eqs. (B3)-(B6), where M and  $r_{\text{c1}}$  are the mass and the scale–lenght of the  $n\text{-}\gamma$  component. As the integration is trivial but the results not particularly illuminating, we do not show the explicit formulae.

### REFERENCES

An, J.H., & Evans, W. 2006, ApJ, 642, 752 (AE06)

Baes, M., & Dejonghe, H. 2004, MNRAS, 351, 18

Baes, M., Dejonghe, H., & Buyle, P. 2005, A&A, 432, 411 Bertin, G. 2000, Dynamics of Galaxies (Cambridge: Cambridge University Press)

Bertin, G., & Stiavelli, M. 1984, A&A, 137, 26

Bertin, G., & Trenti, M. 2003, ApJ, 584, 729

Bertin, G., Saglia, R.P., & Stiavelli, M. 1992, ApJ, 384, 423 Binney, J., & Merrifield, M. 1998, Galactic Astronomy,

(Princeton: Princeton University Press)

Binney, J., & Mamon, G. 1982, MNRAS, 200, 361

Binney, J., & Tremaine, S. 2008, Galactic Dynamics (2nd Ed.; Princeton: Princeton University Press)

de Bruijne, Jos H.J., van der Marel, R.P., & de Zeeuw, P.T. 1996, MNRAS, 282, 909

Buyle, P., Hunter, C., Dejonghe, H. 2007, MNRAS, 375, 773

Carollo, C.M., de Zeeuw, P.T., & van der Marel, R.P. 1995, MNRAS, 276, 1131

Ciotti, L. 1991, A&A, 249, 99

Ciotti, L. 1996, ApJ, 471, 68 (C96)

Ciotti, L. 1999, ApJ, 520, 574 (C99)

Ciotti, L. 2000, Lecture Notes on Stellar Dynamics (Pisa: Scuola Normale Superiore Ed.)

Ciotti, L., & Pellegrini, S. 1992, MNRAS, 255, 561 (CP92)

Ciotti, L., & Lanzoni, B. 1997, A&A, 321, 724

Ciotti, L., Lanzoni, B., & Renzini, A. 1996, MNRAS, 282,

Ciotti, L., & Bertin, G. 2005, A&A, 437, 419

Ciotti, L., Morganti, L., & de Zeeuw, P.T. 2008, MNRAS in press (arXiv:0809.4444)

Cuddeford, P. 1991, MNRAS, 253, 414

Cuesta, A.J., Prada, F., Klypin, A., & Moles, M. 2008, MNRAS, 389, 385

de Vaucouleurs, G. 1948, Ann.d'Ap., 11, 247

Dehnen, W. 1993, MNRAS, 265, 250

Dejonghe, H. 1986, Phys. Rep., 133, No. 3-4, 217

Dejonghe, H. 1987, MNRAS, 224, 13

Eddington, A.S. 1916, MNRAS, 76, 572

Fricke, W. 1952, Astron. Nachr., 280, 193

Hernquist, L. 1990, ApJ, 536, 359

Hiotelis, N. 1994, A&A, 291, 725

Hunter, C., & Qian, E. 1993, MNRAS, 262, 401

King, I. 1966, ApJ, 146, 372

King, I. 1972, ApJl, 174, L123

Lynden Bell, D. 1962, MNRAS, 123, 447

Merritt, D. 1985a, AJ, 90, 1027

Nipoti, C., Londrillo, P., & Ciotti, L. 2002, MNRAS, 332, 901

Nipoti, C., Londrillo, P., & Ciotti, L. 2006, MNRAS, 370, 681

Osipkov, L.P. 1979, Pis'ma Astron.Zh., 5, 77

Richstone, D.O., & Tremaine, S.D. 1984, ApJ, 286, 27

Sersic, J. L. 1968, Atlas de Galaxias Australes, Cordoba, Argentina: Observatorio Astronomico

Tremaine, S.D., Richstone, D.O., Byun, Y.I., Dressler, A., Faber, S.M., Grillmair, C., Kormendy, J., & Lauer, T.R. 1994, AJ, 107, 634

Trenti, M, Bertin, G., & van Albada, T.S. 2005, A&A, 433, 57

van Albada, T.S. 1982, MNRAS, 201, 939

Zhao, H. S. 1996, MNRAS, 278, 488